Acta Mech 224, 139–156 (2013)
DOI 10.1007/s00707-012-0740-y

Cliff Butcher · Zengtao Chen · Michael Worswick

Integration of a particle-based homogenization theory into a general damage-based constitutive model to improve the modelling of void nucleation to coalescence

Received: 3 November 2011 / Revised: 5 September 2012 / Published online: 25 October 2012

Abstract A novel framework and integration scheme has been developed to implement a secant-based homogenization theory for particle-reinforced plasticity into an existing damage-based constitutive model. In this approach, the material is envisaged as a three-phase composite composed of voids and particles embedded in a ductile matrix. Two successive homogenization theories (damage- and particle-based) are then applied to determine the macro-mechanical response of the material as well as the average stress state within the constituents as a function of the particle shape, composition and volume fraction. By identifying the stress state within the particles and the matrix, void nucleation can be accurately represented and the void growth and coalescence models are improved through knowledge of the stress state within the matrix. The performance of this loosely coupled model is analytically evaluated using idealized composite materials that contain inclusions of various shapes to elucidate the influence of the inclusion morphology on damage evolution and coalescence. The present work provides an efficient, albeit approximate, algorithm that can be readily included into existing damage-based constitutive models to improve their predictions of damage evolution, particularly related to void nucleation.

List of symbols

Standard notation is used throughout. All tensor components are defined with respect to the global Cartesian system with the base vectors $\mathbf{e}_i$ $(i = 1, 2, 3)$ and the summation convention is used for repeated indices. A superposed dot indicates the time derivative. Any tensor or quantity associated with the composite matrix is denoted with an overbar symbol and a subscript s denotes a secant quantity.

$a^{(r)}, b^{(r)}$	Stress concentration factors for the hydrostatic and deviatoric stress in the rth phase
$D_{ij}, D_{\text{eq}}, D_1$	Strain tensor, equivalent strain and the maximum principal strain in the damage-based constitutive model
$D^p_{ij}, D^p_{\text{eq}}$	Plastic strain tensor and the equivalent plastic strain in the damage-based constitutive model
$E^{(r)}$	Elastic modulus of the rth phase (GPa)
$\bar{E}$	Elastic modulus of the composite matrix (GPa)

C. Butcher (✉) · M. Worswick
Department of Mechanical and Mechatronics Engineering, University of Waterloo,
Waterloo, ON, N2L 3G1, Canada
E-mail: cliff.butcher@gmail.com; cbutcher@uwaterloo.ca

Z. Chen
Department of Mechanical Engineering, University of New Brunswick,
Fredericton, NB, E3B 5A3, Canada

f_{o}, f	Initial and current porosity (void volume fraction)
$f_{\mathrm{o}}^{(1)}$, $f^{(1)}$	Initial and current volume fraction of the particles
$\dot{f}_{\mathrm{growth}}$	Void growth rate
$\dot{f}_{\mathrm{nucleation}}$	Void nucleation rate
L_{ijkl}	Fourth-order elastic stiffness tensor
L_x, L_y, L_z	Half lengths of the unit cell in the x, y, z directions (m)
$K_{1\mathrm{c}}$	Critical mode 1 fracture toughness (MPa-m$^{1/2}$)
$\bar{n}$	Hardening exponent of the composite matrix
p_{is}	Parameters related to the computation of the secant bulk modulus
q_{1-3}	Tvergaard's calibration parameters for the Gurson model
q_{is}	Parameters related to the computation of the secant shear modulus
R_x, R_y, R_z	Radii of the spheroidal void in the x, y, z directions (m)
S_{ijkl}	Fourth-order Eshelby tensor
s_{N}	Standard deviation of the nucleation stress (MPa)
T	Stress triaxiality ratio
$V^{(1)}$	Average volume of the particles (m^3)
W_o, W	Initial and current aspect ratio of a spheroidal void
$W^{(1)}$	Aspect ratio of a spheroidal particle
W_{N}	Initial aspect ratio of a nucleated spheroidal void

Greek symbols

α	Parameter in the Griffith criterion for mode I fracture
α_n, β_n	Parameters in the void coalescence model
χ	Void spacing ratio (also known as the ligament size ratio)
δ_{ij}	Kronecker delta
$\varepsilon_{ij}^{(r)}$, $\varepsilon_{\mathrm{eq}}^{(r)}$, $\varepsilon_{\mathrm{hyd}}^{(r)}$	Strain tensor, equivalent strain and hydrostatic strain in rth phase
$\varepsilon_{ij}^{p(r)}$, $\varepsilon_{\mathrm{eq}}^{p(r)}$, $\varepsilon_{\mathrm{hyd}}^{p(r)}$	Plastic strain tensor, equivalent plastic strain and hydrostatic plastic strain in rth phase
$\bar{\varepsilon}_{ij}$, $\bar{\varepsilon}_{\mathrm{eq}}$, $\bar{\varepsilon}_{\mathrm{hyd}}$	Strain tensor, equivalent strain and hydrostatic strain in composite matrix
$\bar{\varepsilon}_{ij}^{p}$, $\bar{\varepsilon}_{\mathrm{eq}}^{p}$, $\bar{\varepsilon}_{\mathrm{hyd}}^{p}$	Plastic strain tensor, equivalent plastic strain and hydrostatic plastic strain in composite matrix
ε_{N}	Mean nucleation strain
γ_{cell}	Geometry factor for the unit cell
$\kappa^{(r)}$	Bulk modulus of the rth phase (MPa)
η	Parameter in the void growth model
λ_{o}, λ	Initial and current aspect ratio of the unit cell
$\mu^{(r)}$	Shear modulus of the rth phase (MPa)
$\nu^{(r)}$	Poisson ratio of the rth phase
Φ	Flow potential
Σ_{ij}, Σ_{eq}, Σ_{hyd}	Macroscopic stress tensor, equivalent stress and hydrostatic stress in the damage-based constitutive model (MPa)
$\bar{\sigma}_{ij}$, $\bar{\sigma}_{\mathrm{eq}}$, $\bar{\sigma}_{\mathrm{hyd}}$	Stress tensor, equivalent stress and hydrostatic stress in the composite matrix (MPa)
$\sigma_{ij}^{(r)}$, $\sigma_{\mathrm{eq}}^{(r)}$, $\sigma_{\mathrm{hyd}}^{(r)}$	Stress tensor, equivalent stress and hydrostatic stress in the rth phase (MPa)
σ_{N}	Mean nucleation stress (MPa)
σ^{p}	Equivalent or maximum principal stress in the particle for nucleation modelling
$\bar{\sigma}_{\mathrm{y}}$, $\bar{\sigma}$	(MPa) Yield strength and flow stress of the composite matrix (MPa)
ω	Parameter in the void shape evolution model

1 Introduction

Damage-induced ductile fracture is a complex and highly coupled process that is initiated by the nucleation of microvoids by the cracking or debonding of second-phase particles and inclusions. These voids grow during plastic deformation leading to sudden fracture as the voids coalesce and link-up throughout the material. Great strides have been made in recent years in developing advanced damage-based constitutive models to describe

this fracture mechanism by incorporating physically motivated models for void growth, shape evolution and coalescence [1–11]. However, the development of a physically sound nucleation model remains an open area of research. Accurate modelling of void nucleation is difficult within a damage-based framework such as the well-known Gurson–Tvergaard (GT) [12,13] model due to the intrinsic assumption that the material does not contain any second-phase particles. Consequently, the void nucleation models employed in these constitutive models are overly simplistic as the particle shape, composition, stress state and load sharing are neglected, lumped into a single calibration parameter [14] or indirectly accounted for in a phenomenological manner [15]. Furthermore, the growth and coalescence of existing voids are affected by the presence of second-phase particles that alter the stress state in the material due to load sharing with the matrix. As such, there is a clear need for an efficient, albeit approximate method to account for the role of the particles and inclusions on ductile fracture within a damage-based framework.

The influence of the second-phase particles and inclusions on the overall response of a material can be described using a particle-based homogenization theory. Many types of homogenization techniques have been developed such as secant-based [16–20], tangent-based [21–23], generalized self-consistent [24] and variational approaches [25,26]. Excellent reviews on the efforts to develop particle-based homogenization techniques in the plastic regime can be found in Ponte Casteneda and Suquet [27] and Chaboche et al. [28]. Today, it is generally agreed that both secant and tangent-based homogenization models can provide acceptable approximations to the material behaviour of composite materials in the elastic and plastic regimes [29]. As each type of homogenization model has its advantages, the desired application of the model is perhaps the most important factor in its selection. Mueller and Mortensen [30] evaluated five different homogenization schemes in the plastic regime (secant, self-consistent, generalized self-consistent, differential effective-medium, identical hard spheres approximation) and found no discernible difference in the predictions for the bulk and shear moduli of the composite when the particle content was less than 10 %.

A recent finite-element study by Pierard et al. [24] evaluated a classical secant [19,31], modified secant [20] and tangent-based [23] homogenization models for a material containing aligned ellipsoidal particles with a volume fraction of 30 %. It was revealed that while the incremental and modified secant methods gave the best estimates for the composite stress, the stress within the particles was best predicted using the classical secant method. This is an important result that emphasizes the fact that the ability of a model to predict the overall response of a material from its constituents does not mean that the predicted stress within the constituents is also accurate. These results serve to highlight the approximate nature of the homogenization models and that in many cases, there may not be a distinct advantage in selecting one model over another.

The materials of interest in the present work are industrial alloys such as automotive-grade aluminium–magnesium alloys where the volume fraction of second-phase particles is on the order of a few percent [32]. As such, the reinforcement of these particles on the stress–strain curve is not of prime concern since they are generally not considered at all in Gurson-based constitutive models. The influence of the particles in Gurson-based models is implicitly captured by using the experimental flow stress relation and assuming it describes the behaviour of the virgin matrix. In this work, our interest lies with augmenting existing damage-based constitutive models with the knowledge of the stress state in the inclusions so that physically accurate void nucleation rules can be employed in future applications. Our principal concern is to improve the modelling of void nucleation and evolution and not the prediction of the macroscopic response of the material from its constituents. A secant-based homogenization scheme will be adopted in the present work because they are computationally efficient, easily implemented into numerical codes and can provide reasonable estimations for the stress in the matrix and inclusions. The subsequent sections of this manuscript are organized as follows:

- Development of the integration procedure for implementing the homogenization scheme into a damage-based framework.
- Description of the particle-based homogenization model used in the present work.
- Implementation of the particle-based model into an enhanced GT constitutive model.
- Evaluation and application of the coupled-GT model in several stress states common to sheet metal forming for a model aluminium alloy. The effect of the inclusion shape is investigated.

2 Approximate procedure for integrating a general particle-based homogenization theory into an existing damage-based constitutive model

Consider a bulk material that contains voids and hard elastic particles within a ductile matrix that is subjected to a deformation process (Fig. 1). The influence of the voids on the response of the bulk material can be

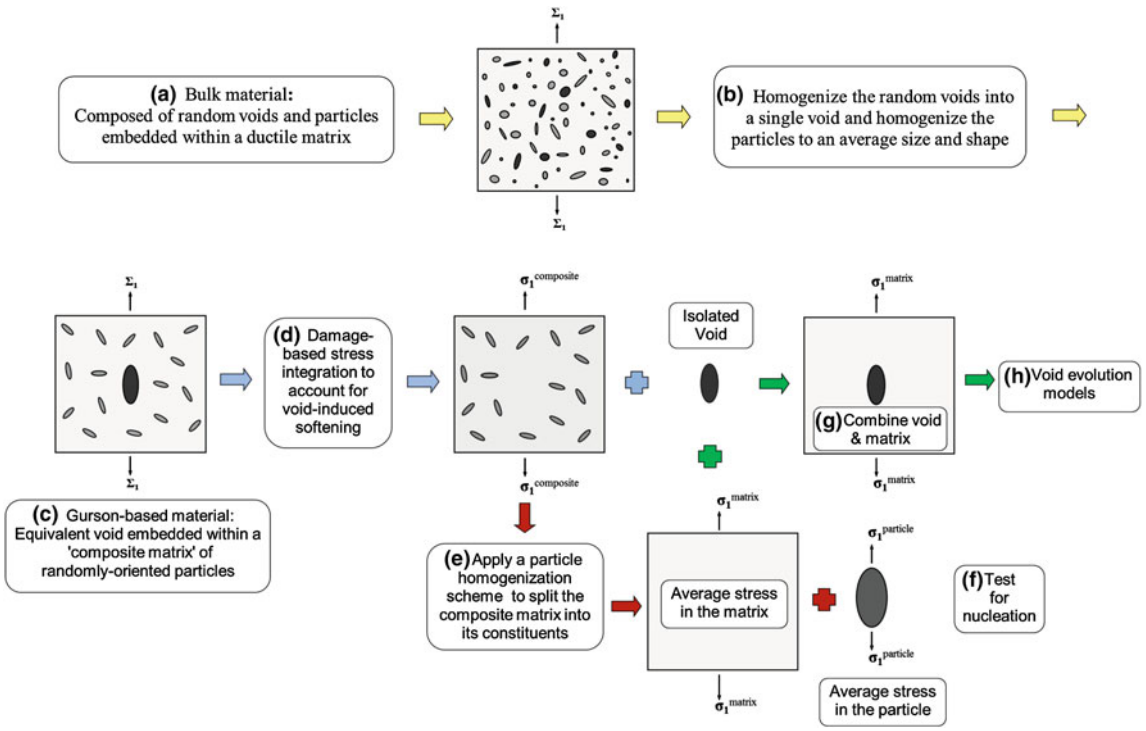

Fig. 1 Schematic of the integration process of a particle-based homogenization theory into a damage-based constitutive model

described using a damage-based constitutive model such as the Gurson model [12]. Gurson-based models are the result of a homogenization procedure for a material composed of voids embedded within a ductile virgin matrix. Therefore, a Gurson-based model can be applied to the bulk material to account for void damage by modelling the bulk material as a material that contains voids embedded within a so-called "*composite matrix*" that is composed of the virgin matrix and the particles. The experimental flow stress relation of the composite matrix can be obtained from a torsion or compression test of the bulk material to mitigate the influence of the voids. A tensile test could also be used if the initial porosity is 0.2 % or lower [9].

The typical procedure for the stress integration of a Gurson-based material model can now be applied to the bulk material. The material has a void volume fraction or porosity, f, and is subjected to a monotonic proportional loading defined by the macroscopic strain tensor, D_{ij}. The stress state is then integrated using the damage-based yield surface to determine the macroscopic stress tensor, Σ_{ij}. The equivalent plastic strain and flow stress within the composite matrix are $D^{\mathrm{p}}_{\mathrm{eq}}$ and $\bar{\sigma} = \bar{\sigma}(D^{\mathrm{p}}_{\mathrm{eq}})$. The stress state is defined by the stress triaxiality ratio, $T = \Sigma_{\mathrm{hyd}}/\Sigma_{\mathrm{eq}}$.

The bulk material is softened by the presence of the voids and thus the composite matrix must work harden to a greater extent to reach the applied strain of D_{ij} than if no voids were present such that $\bar{\sigma} > \Sigma_{\mathrm{eq}}$. Since the voids do not contribute to load sharing, the entire load must be borne by the virgin matrix and the particles. From the perspective of the constituents, this is equivalent to subjecting the composite matrix to a larger applied strain denoted $\bar{\varepsilon}_{ij}$ that results in the same equivalent stress, plastic strain and stress triaxiality as when softening was considered.

The situation for the composite matrix now resembles that of a particle-based homogenization problem for a prescribed traction. The equivalent stress state within the composite matrix is known and the stress state in the constituents must be determined that is in equilibrium with this prescribed stress. A particle-based homogenization method can be employed to determine the effective moduli of the composite matrix that satisfies the stress state defined by the damage-based stress integration. The stress state in the particles can then be used to evaluate a void nucleation model for particle cracking and/or debonding. The stress state in the virgin matrix is used to evaluate the models for void evolution since the voids must obey the plasticity in the matrix. This is a significant contribution as the physical foundations of the void nucleation and evolution models can be strengthened without introducing additional heuristic material parameters that dilute the integrity of the constitutive model.

It is important to note that the interactions between the voids and the particles are not considered in this approach and that these interactions will certainly influence the stress state, particularly within heterogeneous particle and void clusters. However, even mean-field-based particle homogenization schemes underestimate the actual plastic strain in materials with non-dilute concentrations of particles due to the significant local stress and strain gradients that develop in the plastic regime [24]. Consequently, the error introduced by ignoring the void–particle interactions can be lumped into the general uncertainty related to the homogenization scheme. Additionally, void–void interactions are not considered in typical Gurson-based constitutive models although non-local averaging techniques have been proposed to account for this deficiency [32].

Overall, the proposed integration scheme can be applied to any composite material but from a physical standpoint, it is best suited for materials containing dilute concentrations of particles and voids in order to mitigate the influence of particle–particle, particle–void and void–void interactions. A suggested guideline for the maximum particle content would be 20 %. An upper limit for the porosity is not required since the porosity at failure is normally on the order of several percent or less [9]. Advanced constitutive models are available in the literature that can better account for both voids and particles such as the variational model of Kailasam and Ponte Casteneda [26]. However, the motivation for this work is to improve the physical foundation of the commonly used Gurson-based damage models by accounting for the influence of the particles while retaining the recent advances in the modelling of ductile fracture.

3 Integration of the particle-based homogenization scheme into a damage-based constitutive model

3.1 Particle homogenization scheme

The particle-based homogenization scheme considered in this work was developed by Tandon and Weng [18] for a dual-phase composite subjected to a prescribed traction. The composite is composed of randomly oriented elastic particles embedded within a ductile matrix as shown in Fig. 1. The particles are spheroidal and characterized by their elastic properties, volume fraction and aspect ratio (length-to-diameter). This model is valid for inclusion shapes ranging from flat discs to ellipsoids and elongated fibres. This homogenization model employs a secant-based approach that utilizes Berveiller and Zaoui's [16] modification to the solution of Hill [21] for proportional loading and incorporates the mean-field method of Mori and Tanaka [31] to account for particle-particle interactions. Additional details of the derivation of this model can be found in [18] and this section will only present the theory relevant for integration with a damage-based constitutive model.

The ductile virgin matrix material is treated as phase 0 and the embedded elastic particles are defined as phase 1 with a volume fraction, $f^{(1)}$, and aspect ratio, $W^{(1)}$. The respective isotropic Poisson's ratio, and bulk, shear and elastic moduli of the rth phase are denoted by $v^{(r)}$, $\kappa^{(r)}$, $\mu^{(r)}$ and $E^{(r)}$ with a subscript, s, used to denote a secant quantity such as the secant shear modulus of the matrix, $\mu_s^{(0)}$. The stress and strain tensors for the rth phase are denoted by $\sigma_{ij}^{(r)}$ and $\varepsilon_{ij}^{(r)}$ which can be decomposed into their respective deviatoric and hydrostatic components as $\sigma_{ij}^{(r)} = \sigma_{ij}^{\prime(r)} + \delta_{ij}\sigma_{\text{hyd}}^{(r)}$ with $\sigma_{\text{hyd}}^{(r)} = \sigma_{kk}^{(r)}/3$ and $\varepsilon_{ij}^{(r)} = \varepsilon_{ij}^{\prime(r)} + \delta_{ij}\varepsilon_{\text{hyd}}^{(r)}$ with $\varepsilon_{\text{hyd}}^{(r)} = \varepsilon_{kk}^{(r)}/3$, where δ_{ij} is the Kronecker delta. The behaviour of the two-phase composite in the particle-based homogenization model describes the behaviour of the composite matrix in the damage-based constitutive model. Any property or quantity associated with the composite is denoted using an overbar symbol such as $\bar{\sigma}_{ij}$ for the stress tensor of the composite matrix.

In a composite material, the constituents are generally in a triaxial state of stress that should be characterized using the equivalent measures for the stress, strain and plastic strain as follows:

$$\sigma_{\text{eq}}^{(r)} = \sqrt{(3/2)\,\sigma_{ij}^{\prime(r)}\sigma_{ij}^{\prime(r)}}, \tag{1}$$

$$\varepsilon_{\text{eq}}^{(r)} = \sqrt{(2/3)\,\varepsilon_{ij}^{\prime(r)}\varepsilon_{ij}^{\prime(r)}}, \tag{2}$$

$$\varepsilon_{\text{eq}}^{p} = \sqrt{(2/3)\,\varepsilon_{ij}^{p}\varepsilon_{ij}^{p}}. \tag{3}$$

The components of the stress and strain in the composite are related through the effective secant shear and bulk moduli as:

$$\bar{\sigma}'_{ij} = 2\bar{\mu}_s \bar{\varepsilon}'_{ij} \qquad \bar{\sigma}_{\text{hyd}} = 3\bar{\kappa}_s \bar{\varepsilon}_{\text{hyd}}. \tag{4a, b}$$

To determine the stress and strain in the composite and its constituents during plastic deformation, the effective secant elastic moduli of the matrix and composite must first be determined as functions of the matrix plastic strain, $\varepsilon_{\text{eq}}^{\text{p}(0)}$. The secant elastic modulus and Poisson's ratio of the matrix can be expressed as:

$$E_s^{(0)} = \frac{1}{1/E^{(0)} + \varepsilon_{\text{eq}}^{\text{p}(0)}/\sigma_{\text{eq}}^{(0)}} = \frac{3E^{(0)}\mu_s^{(0)}}{E^{(0)} + \mu_s^{(0)}(1 - 2v^{(0)})}, \tag{5}$$

$$v_s^{(0)} = \frac{1}{2} - \left(\frac{1}{2} - v^{(0)}\right)\frac{E_s^{(0)}}{E^{(0)}}. \tag{6}$$

The secant bulk and shear moduli are obtained using the standard isotropic relations $\mu_s^{(0)} = E_s^{(0)}/2(1 + v_s^{(0)})$ and $\kappa_s^{(0)} = E_s^{(0)}/3(1 - 2v_s^{(0)})$. The matrix material is assumed to be plastically incompressible and thus the secant bulk modulus remains constant at $\kappa_s^{(0)} = \kappa^{(0)}$. The effective secant moduli of the composite material can be determined as:

$$\bar{\kappa}_s = \frac{\kappa_s^{(0)}}{1 + f^{(1)} p_{2s}/p_{1s}}, \tag{7}$$

$$\bar{\mu}_s = \frac{\mu_s^{(0)}}{1 + f^{(1)} q_{2s}/q_{1s}}, \tag{8}$$

where p_{is} and q_{is} are the functions of the particle shape, volume fraction, elastic moduli of the constituents and the fourth-order Eshelby [33] S tensor. The expressions for p_{is} and q_{is} are lengthy and are not presented here for brevity but can be found in [18].

3.2 Average stress in the composite and its constituents

The respective hydrostatic and deviatoric stresses in each constituent are determined from the composite stress tensor using the stress concentration factors, $a^{(r)}$ and $b^{(r)}$

$$\sigma_{\text{hyd}}^{(r)} = a^{(r)}\bar{\sigma}_{\text{hyd}} \qquad \sigma_{ij}^{\prime(r)} = b^{(r)}\bar{\sigma}'_{ij} \qquad \sigma_{eq}^{(r)} = b^{(r)}\bar{\sigma}_{eq}, \tag{9a–c}$$

$$a^{(0)} = 1/p_{1s} \qquad a^{(1)} = \left(1 - (1 - f^{(1)})a^{(0)}\right)/f^{(1)},$$

$$b^{(0)} = 1/q_{1s} \qquad b^{(1)} = \left(1 - (1 - f^{(1)})b^{(0)}\right)/f^{(1)}. \tag{10a–d}$$

The stress in the composite and its constituents must be in equilibrium and thus:

$$\bar{\sigma}_{ij} = (1 - f^{(1)})\sigma_{ij}^{(0)} + f^{(1)}\sigma_{ij}^{(1)}. \tag{11}$$

The onset of yielding of the matrix occurs when $\bar{\sigma}_{\text{eq}} \geq \sigma_{\text{y}}^{(0)}/b^{(0)}$ with $b^{(0)}$ determined using the elastic moduli of the matrix in Eqs. (5) and (6).

3.3 Average strain in the composite and its constituents

Due to the presence of the elastic inclusions, the composite is not plastically incompressible and the composite plastic strain tensor must be determined from the elastic unloading process as:

$$\bar{\varepsilon}_{ij}^{p} = \left(\frac{1}{2\bar{\mu}_s} - \frac{1}{2\bar{\mu}}\right)\bar{\sigma}'_{ij} + \delta_{ij}\left(\frac{1}{3\bar{\kappa}_s} - \frac{1}{3\bar{\kappa}}\right)\bar{\sigma}_{\text{hyd}}. \tag{12}$$

The matrix is assumed to be isotropic and obey J_2 plasticity (von Mises material), from which the plastic strain components can be readily determined by integrating the J_2 flow rule for proportional loading to yield:

$$\varepsilon_{ij}^{p}(0) = \frac{3}{2}\frac{\varepsilon_{\text{eq}}^{\text{p}(0)}}{\bar{\sigma}}\bar{\sigma}'_{ij}. \tag{13}$$

The particles are assumed to remain elastic during deformation and the strain in the particles can be expressed as:

$$\varepsilon_{ij}^{(1)} = \frac{b^{(1)}\bar{\sigma}'_{ij}}{2\mu^{(1)}} + \delta_{ij}\frac{a^{(1)}\bar{\sigma}_{\text{hyd}}}{3\kappa^{(1)}}. \tag{14}$$

The solution for the secant moduli of the composite and subsequent stress and strain in the constituents is non-linear and an iterative solution is required in the plastic regime. The required material parameters to determine the behaviour of the composite and stress in the constituents are $E^{(0)}$, $v^{(0)}$, $E^{(1)}$, $v^{(1)}$, $f^{(1)}$ and $W^{(1)}$. A simple fixed-point algorithm can be implemented to determine the required value for $\varepsilon_{\text{eq}}^{\text{p}(0)}$ and is described in Tandon and Weng [18]. However, this solution method must be modified in the present work because this particle-based homogenization method is to be coupled with a damage-based constitutive model to account for the influence of the voids on the subsequent stress and strain in the constituents.

3.4 Stress state in the composite matrix

To create a stress state in the composite matrix equivalent to the stress state of the voided bulk material, the applied composite matrix strain tensor, $\bar{\varepsilon}_{ij}$, must be determined to produce a composite stress tensor, $\bar{\sigma}_{ij}$, subject to the constraints that the stress state is equivalent: $\bar{\sigma}_{\text{eq}} = \bar{\sigma}$, $\bar{\sigma}_{\text{hyd}}/\bar{\sigma}_{\text{eq}} = T$ and $\bar{\varepsilon}_{\text{eq}}^{p} = D_{\text{eq}}^{p}$. The procedure to determine $\bar{\varepsilon}_{ij}$ and $\bar{\sigma}_{ij}$ using a secant-based homogenization scheme for monotonic, proportional loading is described using the following procedure.

First, the hydrostatic stress of the composite matrix can be computed directly from the requirement of an equivalent triaxiality ratio as

$$\bar{\sigma}_{\text{hyd}} = \bar{\sigma}(\Sigma_{\text{hyd}}/\Sigma_{\text{eq}}). \tag{15}$$

From the definition of the effective secant moduli in Eq. (4a, b) and the equivalent stress and strain in Eqs. (1) and (2), the equivalent strain in the composite matrix is

$$\bar{\varepsilon}_{\text{eq}} = \bar{\sigma}/3\bar{\mu}_s. \tag{16}$$

Only the deviatoric stress and strain components of the composite matrix remain unknown and only one is required to be pre-determined because they are related through the secant shear modulus. The deviatoric strain in the composite is assumed to be proportional to the applied deviatoric strain in the damage-based model using the relation

$$\bar{\varepsilon}'_{ij} = \xi D'_{ij}, \tag{17}$$

so that $\xi = \bar{\varepsilon}_{\text{eq}}/\bar{D}_{\text{eq}}$, and the stress and applied strain tensors of the composite matrix can be obtained as

$$\bar{\sigma}_{ij} = \left(\frac{2}{3}\frac{\bar{\sigma}}{D_{\text{eq}}}\right)D'_{ij} + \delta_{ij}\bar{\sigma}_{\text{hyd}}, \tag{18}$$

$$\bar{\varepsilon}_{ij} = \left(\frac{1}{3\bar{\mu}_s}\frac{\bar{\sigma}}{D_{\text{eq}}^{p}}\right)D'_{ij} + \delta_{ij}\frac{\bar{\sigma}_{\text{hyd}}}{3\bar{\kappa}_s}, \tag{19}$$

which satisfies the requirements for an equivalent stress state such that $\bar{\sigma}_{\text{hyd}}/\bar{\sigma}_{\text{eq}} = T$ and $\bar{\sigma}_{\text{eq}} = \bar{\sigma}$. The stress tensor of the composite matrix can be evaluated immediately following the stress integration of the damage-based constitutive model while $\bar{\varepsilon}_{ij}$ requires knowledge of the effective secant moduli which have yet to be determined.

3.5 Iterative solution for the effective secant moduli of the composite matrix

An iterative procedure is required to determine the effective secant moduli of the composite matrix from which the stress and strain within the constituents can be determined. The iterative solution is developed from the constraint that the secant elastic moduli must result in the same plastic strain in the composite matrix as dictated from the damage-based stress integration: $\bar{\varepsilon}^p_{\text{eq}} = D^p_{\text{eq}}$. The plastic strain of the composite matrix must account for the elastic heterogeneity of the particles, and from substituting Eq. (12) into Eq. (3) and utilizing Eq. (1), the required secant shear modulus of the composite matrix is

$$\bar{\mu}^*_s = \frac{\bar{\mu}\bar{\sigma}}{\bar{\sigma} + \bar{\mu}\sqrt{(3D^p_{\text{eq}})^2 - 2\,(1/\bar{\kappa}_s - 1/\bar{\kappa})^2\,\bar{\sigma}^2_{\text{hyd}}}}. \tag{20}$$

All of the parameters in Eq. (20) are constant during the iteration loop except for the secant bulk modulus, $\bar{\kappa}_s$, that varies with the plastic strain of the matrix, $\varepsilon^{\text{p(0)}}_{\text{eq}}$.

A fixed-point algorithm is used to obtain the solution to the non-linear equations for the secant moduli by iterating upon the secant elastic modulus of the matrix, $E^{(0)}_s$. A trial value for $E^{(0)}_s$ is assumed from which the subsequent trial values for the secant shear, bulk and Poisson's ratios of the matrix can be determined from Eqs. (5) and (6) and used to evaluate the expressions for p_{is} and q_{is}, as well as $\bar{\kappa}_s$ in Eq.(7) and $\bar{\mu}^*_s$ in Eq.(20). A new estimate for $\mu^{(0)}_s$ can be determined by setting $\bar{\mu}_s = \bar{\mu}^*_s$ in Eq. (8) and evaluating Eq. (5) to obtain a new estimate for$E^{(0)}_s$. If this new value of $E^{(0)}_s$ is equal to the trial value, the solution has been obtained, otherwise the algorithm is repeated using the current $E^{(0)}_s$ as the new trial value. Upon convergence, the stress concentration factors to determine the stress and strain tensors of the matrix and particles can be evaluated using Eqs. (9a–c), (13) and (14). This algorithm generally achieves convergence within three iterations to a tolerance of 0.001 and is straightforward in its implementation. A valuable by-product of this integration scheme is that no previous knowledge of the flow stress response of the virgin matrix is required since it can be computed as a fraction of the flow stress response of the composite matrix using Eqs. (9a–c) and Eqs. (10a–d) for a converged solution.

4 Constitutive modelling of ductile fracture

The integration of a homogenization scheme into a Gurson-based damage framework improves all aspects of the damage model and provides a coupling between the various damage mechanisms that are often considered independently. The advantages of the proposed coupled damage-based constitutive model are:

- Modelling of void nucleation is improved through knowledge of the stress state within the particles as a function of their shape, content and composition.
- The stress state within particles becomes progressively more severe as the particle content decreases due to nucleation. This promotes additional nucleation, void growth and material softening.
- The plastic strain and triaxiality within the matrix material is higher than in the composite matrix and thus promotes void evolution and coalescence.
- The flow stress relation of the virgin matrix material does not have to be predetermined.
- The model reverts to its original GT formulation if the material does not contain any inclusions. The GT model reverts to a J_2 material if no voids are present.
- An absolute minimum number of new parameters has been introduced into the damage-based framework. The elastic properties of the constituents as well as the average particle shape and content are typically known from standard material characterization techniques.
- The particle-based homogenization scheme is computationally efficient and readily implemented into any other existing Gurson-type constitutive model.

The proposed integration procedure will now be implemented into an enhanced version of the well-known Gurson–Tvergaard [12,13] constitutive model. A limitation of using a secant-based homogenization scheme is the intrinsic assumption of monotonic proportional loading. As such, the constitutive model is presented using a total-strain formulation.

4.1 Gurson–Tvergaard material model

The Gurson–Tvergaard (GT) model [12,13] is a well-known damage-based constitutive model to describe a porous ductile material containing spherical voids. Ragab [34] extended the model to account for ellipsoidal voids by developing semi-empirical equations for the calibration parameters q_1 and q_2 as a function of the stress triaxiality, hardening exponent, $\bar{n}$, and the void aspect ratio, W. Other Gurson-type constitutive models which account for void shape effects in a more rigorous manner have been proposed in the literature [3,4,6–10]. The GT yield criterion is

$$\Phi = \frac{\Sigma_{\text{eq}}^2}{\bar{\sigma}^2} + 2fq_1 \cosh\left(q_2 \frac{3}{2}\frac{\Sigma_{\text{hyd}}}{\bar{\sigma}}\right) - q_1^2 f^2 - 1 = 0, \tag{21}$$

where f is the porosity or void volume fraction and the GT formulation reduces to the von Mises yield criterion when $f = 0$ in Eq. (21). The semi-empirical equations of Ragab [34] for the variation of the q_i parameters are valid for a large range of stress triaxiality from $1/3 \leq T \leq 8/3$, and for hardening exponents of $0 \leq \bar{n} \leq 0.4$. The q_i relations are:

$$q_1 = A + BT + CT^2 + DT^3, \tag{22}$$

$$A = 2.28 - 3.55\bar{n} + 3.84\bar{n}^2 \quad B = -0.92 + 1.32\bar{n} - 0.32\bar{n}^2,$$
$$C = 0.53 - 2.31\bar{n} + 2.35\bar{n}^2 \quad D = -0.10 + 0.27\bar{n} + 0.70\bar{n}^2 - 1.78\bar{n}^3,$$

$$q_2 = W^{\eta}, \tag{23}$$

$$\eta(W < 1) = 0.206\ln(T) - 0.266 - 0.02\bar{n},$$
$$\eta(W \geq 1) = -3.484 + 11.614T - 13.72T^2 + 6.54T^3 - 1.06T^4 + 0.2\bar{n}.$$

4.2 Degradation of the elastic moduli

The void-induced degradation of the initial shear and bulk modulus ($\bar{\mu}_{\text{o}}$, $\bar{\kappa}_{\text{o}}$) of the composite matrix is approximated using the Mori–Tanaka solution [31] for spherical voids as

$$\bar{\kappa} = \frac{4(1-f)\bar{\kappa}_{\text{o}}\bar{\mu}\text{o}}{4\bar{\mu}_{\text{o}} + 3f\bar{\kappa}_{\text{o}}}, \tag{24}$$

$$\bar{\mu} = \frac{(1-f)\bar{\mu}_{\text{o}}}{1 + f(6\bar{\kappa}_{\text{o}} + 12\bar{\mu}_{\text{o}})/(9\bar{\kappa}_{\text{o}} + 8\bar{\mu}_{\text{o}})}. \tag{25}$$

4.3 Void growth

The associated flow rule of the GT model yields the following expression for the void growth rate:

$$\dot{f}_{\text{growth}} = \frac{3f(1-f)q_1q_2 \sinh\left(q_2\frac{3}{2}\frac{\sigma_{\text{hyd}}^{(0)}}{\sigma_{\text{eq}}^{(0)}}\right)}{3\left(\frac{\sigma_1^{(0)} - \sigma_{\text{hyd}}^{(0)}}{\sigma_{\text{eq}}^{(0)}}\right) + fq_1q_2 \sinh\left(q_2\frac{3}{2}\frac{\sigma_{\text{hyd}}^{(0)}}{\sigma_{\text{eq}}^{(0)}}\right)}\dot{\varepsilon}_1^{\text{p}(0)}, \tag{26}$$

where $\sigma_1^{(0)}$ and $\dot{\varepsilon}_1^{\text{p}(0)}$ are the first principal stress and plastic strain rate of the virgin matrix. The relation in Eq. (26) is expressed in terms of $\dot{\varepsilon}_1^{\text{p}(0)}$to enable the computation of void growth using the stress state in the virgin matrix instead of the composite matrix.

4.4 Void shape evolution

For a constant strain path, the evolution law for the void aspect ratio is [34]

$$\ln\left(W/W_{\mathrm{o}}\right) = 1.1\left(\omega + 2 - \sigma_{\mathrm{hyd}}^{(0)}/\sigma_{\mathrm{eq}}^{(0)} + \bar{n}\right)\left(1 - f_{\mathrm{o}}\right)\left(\varepsilon_{\mathrm{eq}}^{p(0)} - \varepsilon_{\mathrm{N}}\right), \tag{27}$$

where ε_{N} is the matrix strain at nucleation; f_{o} is the initial porosity; W_{o} is the initial void aspect ratio and ω is defined for oblate ($1/6 \leq W_{\mathrm{o}} \leq 1$) and prolate voids ($1 \leq W_{\mathrm{o}} \leq 6$) as:

$$\omega_{\mathrm{oblate}} = -\ln(W_{\mathrm{o}})\left[0.11 + 1.22(\varepsilon_{\mathrm{eq}}^{\mathrm{p}(0)} - \varepsilon_{\mathrm{N}})\right]^{-1} \quad \omega_{\mathrm{prolate}} = \ln(W_{\mathrm{o}})\left[-0.535 + 0.0235(\varepsilon_{\mathrm{eq}}^{\mathrm{p}(0)} - \varepsilon_{\mathrm{N}})\right]. \tag{28a,b}$$

4.5 Void coalescence

A robust void coalescence criterion has been developed by Thomason [35] to predict the onset of internal necking coalescence between two adjacent voids as a function of the microstructure geometry and stress state. Zhang and Niemi [1,2] were the first to recognize the potential of Thomason's criterion and implemented it into the Gurson–Tvergaard model to predict coalescence, thus removing the critical porosity as a material parameter. Several extensions to this model have been proposed to account for hardening, flat voids and dual populations of voids [4–6,8,10]. For a periodic arrangement of axisymmetric (cylindrical) unit cells, the onset of coalescence occurs when the following condition is satisfied:

$$\frac{\sigma_1^{(0)}}{\sigma_{\mathrm{eq}}^{(0)}} \geq \left(\alpha_n(\bar{n})\left(\frac{1-\chi}{W\chi}\right)^2 + \frac{\beta_n(\bar{n})}{\sqrt{\chi}}\right)\left(1-\chi^2\right), \tag{29}$$

where α_n and β_n are the calibration constants determined by Pardoen and Hutchinson [4] as $\alpha_n = 0.1 + 0.22\bar{n} + 4.8\bar{n}^2$ and $\beta_n = 1.24$; χ is the void spacing ratio and λ is the aspect ratio of the unit cell. The void spacing ratio is defined as the ratio of the lateral void radius to the lateral void spacing for a periodic arrangement of unit cells as shown in Fig. 2. The void spacing and cell aspect ratios evolve with the microstructure during deformation according to the following equations:

$$\chi = \frac{R_y}{\sqrt{L_x L_z}} = \left(\frac{f}{\gamma_{\mathrm{cell}}}\frac{\lambda}{W}\right)^{1/3}, \tag{30}$$

$$\lambda = \frac{L_y}{\sqrt{L_x L_z}} = \lambda_{\mathrm{o}} \exp\left(\frac{3}{2}D_1\right). \tag{31}$$

The parameter γ_{cell} is specific to the assumed unit cell geometry with $\gamma_{\mathrm{cell}} = 2/3$ for the axisymmetric unit cell used in the present work.

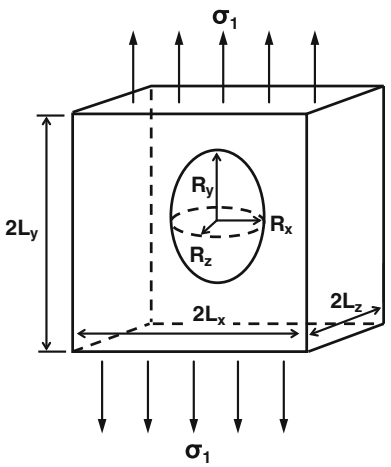

Fig. 2 Cubic unit cell containing an axisymmetric elliptical void ($R_x = R_z$) subjected to uniaxial loading

Table 1 Material parameters of the constituents in the model material

Constituent	Material parameters
Composite matrix	$\bar{\sigma}_y = 150\,\text{MPa}$ $\bar{n} = 0.17$ $\bar{E} = 71.1\,\text{GPa}$ $\bar{\nu} = 0.29$
Matrix	$E^{(0)} = 69\,\text{GPa}$ $\nu^{(0)} = 0.30$
Particles	$E^{(1)} = 90\,\text{GPa}$ $\nu^{(1)} = 0.17$ $f_o^{(1)} = 10\,\%$ $W_o^{(1)} =$ varied parametrically
Voids	$f_o = 0.1\,\%$ $W_o = 1/6$ $\lambda_o = 10$

5 Application and evaluation of the full constitutive model in plane-stress loading

The enhanced GT constitutive model is applied to a generic model material that is subjected to proportional plane-stress loading to represent a sheet metal forming operation. The composite model material is loosely based upon an aluminium–magnesium alloy from Tohgo and Mochizuki [36] with the material parameters presented in Table 1. The void-related parameters are typical values and arbitrarily assumed to obtain general qualitative trends of performance of the model. The voids are assumed to be pre-existing within the bulk material (no nucleation) and the aspect ratio of the unit cell was taken as $\lambda = 10$, so that the voids are reasonably close together and coalescence can occur within a reasonable strain level. If coalescence does not occur by a large strain of 200 %, the simulation is terminated since coalescence is unlikely to ever occur for that void geometry and stress state.

The average particle shape of the model material is varied to evaluate the role of the inclusion shape on the performance of the enhanced GT model. A nucleation rule is not considered at present since the objective is to demonstrate the ability of the model to predict the stress within the inclusions and matrix and the corresponding impact of the particles on void evolution and coalescence. Consequently, the following trends for void evolution and coalescence are compared relative with the results of the standard GT model. This is an important first step in understanding the behaviour of the enhanced GT model that accounts for the second-phase particles. No effort is made here to calibrate the material parameters to achieve fracture strains in accordance with experiment data since the calibration process can arbitrarily compensate for the shortcomings of the models. For instance, the standard GT model with the weaker physical basis can be calibrated via its nucleation rule to obtain fracture strains in accordance with the enhanced GT model that has the stronger physical foundation. For a specific material, the nucleation rule can easily be added into the model to account for the dominant nucleation mode as recently done by Butcher [32].

The bulk material is subjected to proportional loading where the major and minor true strain increments are related using the load ratio, $\rho = \dot{D}_2/\dot{D}_1$, with ratios of -0.5, 0 and 1 corresponding to uniaxial tension ($T = 1/3$), plane-strain ($T = 1/\sqrt{3}$) and equal-biaxial tension ($T = 2/3$). The flow stress relation for the composite matrix is of the form

$$\bar{\sigma}/\bar{\sigma}_y = \left(1 + \left(\bar{E}/\bar{\sigma}_y\right) D_{eq}^p\right)^{\bar{n}} \quad \text{for} \quad \bar{\sigma} \geq \bar{\sigma}_y. \tag{32}$$

The equations of the full constitutive model have been implemented into a C++ code and evaluated using an applied major strain increment of 0.001. The stress is integrated in the GT damage model using the forward-Eulerian integration scheme of Worswick and Pelletier [37].

6 Results

6.1 Average stress states in the constituents and their implications on the modelling of void nucleation

The coupled damage-based constitutive model naturally separates the stress state of the bulk material containing the particles, voids and matrix into its constituents as shown in Fig. 3. The influence of the voids is embedded within the response of the composite matrix whose stress is known from the GT stress integration. The addition of the particle-based homogenization model into the GT framework enables the application of a stress-based nucleation rule to predict particle cracking or debonding. Stress-based nucleation models have the advantage of being path independent compared with strain-based nucleation models, facilitating the determination of unique nucleation parameters through calibration with experiment data [38].

When modelling nucleation, knowledge of the maximum principal stress is of prime importance as the hard elastic particles may experience a brittle-type fracture or debond in the principal loading direction.

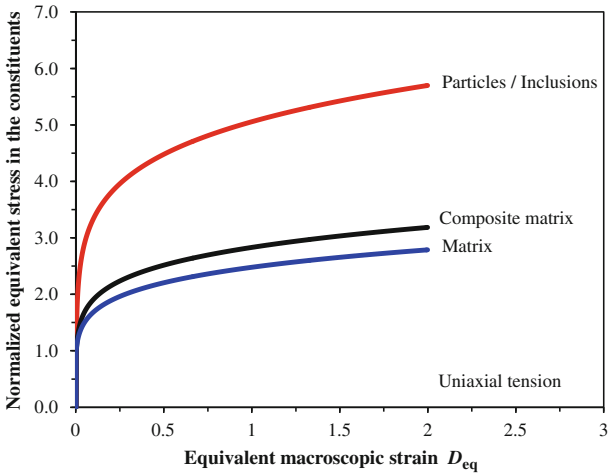

Fig. 3 Equivalent stress within the constituents of the voided bulk material when subjected to uniaxial tension. The inclusions are spherical and the voids are initially oblate. The stress has been normalized by the yield stress of the composite matrix. Note that the particles remain elastic and show a similar trend with the matrix material since its stress response is plotted with the macroscopic equivalent strain

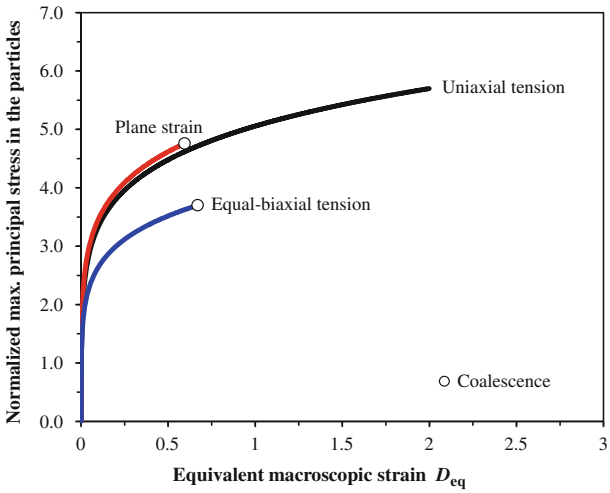

Fig. 4 Normalized maximum principal stress within the spherical elastic particles/inclusions for three loading conditions. The bulk material ruptures due to void coalescence when loaded in plane-strain and equal-biaxial tension while coalescence never occurs in uniaxial tension. The stress has been normalized by the yield stress of the composite matrix. Note that the particles remain elastic and show a similar trend with the matrix material since its stress response is plotted with the equivalent macroscopic strain

The maximum principal stress for any particle shape, composition and stress state is automatically determined within the coupled model as shown in Fig. 4 for several loading conditions. For particle cracking, nucleation is most likely to occur in plane strain as deformation of the material is more constrained resulting in a higher principal stress in the particles. Equal-biaxial tension may favour particle decohesion as the hydrostatic stress in the particles is higher and is being stretched equally in two directions. Using the present approach, the nucleation mechanism will be a natural consequence of the particle geometry and the stress state, paving the way for the adoption of physically realistic nucleation models that can describe these mechanisms such as the interface separation law of Needleman [39]. For example, the stress-based version of the Chu and Needleman [15] nucleation criterion is:

$$\dot{f}_{\text{nucleation}}(f^{(1)}, \Sigma_{ij}, W_{\text{N}}, \sigma_{\text{N}}, s_{\text{N}}) = \frac{W_{\text{N}} f_{\text{n}}}{s_{\text{N}} \bar{\sigma}_{\text{y}} \sqrt{2\pi}} \exp\left[-\frac{1}{2}\left(\frac{\Sigma_{\text{eq}} + \Sigma_{\text{hyd}} - \sigma_{\text{N}}}{s_{\text{N}} \bar{\sigma}_{\text{y}}}\right)^2\right] \left(\dot{\Sigma}_{\text{eq}} + \dot{\Sigma}_{\text{hyd}}\right), \quad (33)$$

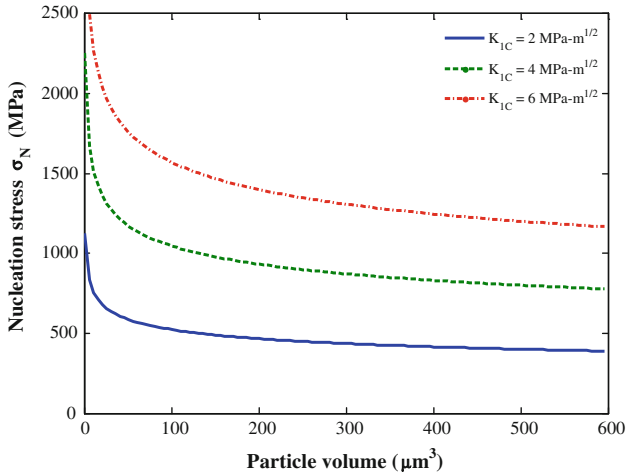

Fig. 5 Variation of the nucleation stress in Eq. (35) with the particle size and fracture toughness

where f_{n} is the volume fraction of void nucleating particles and the stress in the particle is roughly approximated from the macroscopic stresses as $\sigma_{\mathrm{p}} = \Sigma_{\mathrm{eq}} + \Sigma_{\mathrm{hyd}}$. The aspect ratio of the void at nucleation, W_{N}, has been introduced into the model based on the finite-element study of Lassance et al. [8]. For particle cracking, $W_{\mathrm{N}} \leq 0.01$ can accurately represent the formation of a penny-shaped crack while $W_{\mathrm{N}} = W^{(1)}$ is a good estimate for nucleation by complete debonding [7].

In the present work, the stress in the particles is directly computed and thus all of the particles have the potential to nucleate voids, $f_{\mathrm{n}} = f^{(1)}$. The nucleation criterion in Eq. (33) can be reformulated as:

$$\dot{f}_{\mathrm{nucleation}}(f^{(1)}, W^{(1)}, \mu^{(1)}, \kappa^{(1)}, \Sigma_{ij}, W_{\mathrm{N}}, \sigma_{\mathrm{N}}, s_{\mathrm{N}}) = \frac{W_N f^{(1)}}{s_{\mathrm{N}} \bar{\sigma}_{\mathrm{y}} \sqrt{2\pi}} \exp\left[-\frac{1}{2}\left(\frac{\sigma^{\mathrm{p}} - \sigma_{\mathrm{N}}}{s_{\mathrm{N}} \bar{\sigma}_{\mathrm{y}}}\right)^2\right] \dot{\sigma}^{\mathrm{p}}, \tag{34}$$

where σ_{p} can be either the equivalent stress in the particles for general nucleation modelling or the maximum principal stress in the particles to better represent particle cracking. The yield stress of the composite material, $\bar{\sigma}_{\mathrm{y}}$, is simply a normalizing factor and could be replaced by the particle yield stress if it is known. The stress in the particles will evolve as the particles nucleate voids, increasing the stress in the remaining particles and promoting nucleation. Furthermore, the determination of the mean nucleation stress, σ_{N}, through calibration with experiment data will have a stronger physical foundation than using the model in Eq. (33) since the stress in the particles was determined as a function of the global stress state and the particle morphology.

If the dominant nucleation mechanism is particle cracking, the fracture criterion of Moulin et al. [40] for particle break-up during a rolling operation can be employed with slight modification. Moulin et al. [40] observed that the second-phase particles and inclusions in materials contain many surface cracks and internal defects that promote cracking during deformation. Using the Griffith criterion [41] for mode I cracks and performing a rigorous finite-element investigation of the stress states in irregularly shaped inclusions, Moulin et al. [41] developed a criterion based upon the particle volume and the stress distribution within the most deformed regions of the particles.

Fortunately, since the particles are assumed to be ellipsoidal in the present work, the stress distribution inside the particles is uniform according to the solution of Eshelby [33] and the criterion of [41] can be reformulated to obtain an estimate for the nucleation stress as:

$$\sigma_{\mathrm{N}} = \frac{1}{\sqrt{\pi}} \frac{K^*_{1\mathrm{c}}}{\sqrt[6]{V^{(1)}}} \quad K^*_{1\mathrm{c}} = K^{(1)}_{1\mathrm{c}} \sqrt{\alpha} \quad \alpha \approx 1, \tag{35}$$

where K^*_{1C} is the effective critical toughness of the particle material, $V^{(1)}$ is the average particle volume and α is a geometry parameter in the Griffith criterion to account for various effects such as crack blunting. The K_{1c} value can be estimated if the composition of the particle is known or else it can be identified by calibrating the effective K^*_{1C} with the experimental nucleation data. A realistic range for the value of K_{1c} for brittle materials is 1–10 MPa $\cdot \mathrm{m}^{1/2}$ [40]. The geometry factor, α, does not have to be determined and can be lumped into the K^*_{1C} value. The variation of the particle nucleation stress with the volume is presented in Fig. 5. The criterion

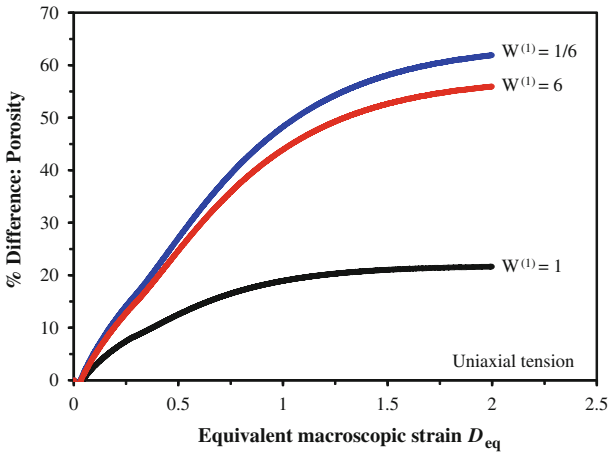

Fig. 6 Influence of the particle shape on damage development in the coupled constitutive model compared with the porosity determined using the standard model. The trends are similar for plane-strain and equal-biaxial tensile loading

captures the particle size effect where small particles nucleate at high strains while large particles nucleate at low stresses and are roughly independent of the particle size [35]. The nucleation model also predicts that brittle phases are more likely to crack than more ductile phases.

The only remaining parameter to be identified in the nucleation criterion in Eq. (34) is the standard deviation of the nucleation stress, s_N. The standard deviation of the particle volume distribution would likely provide a reasonable estimate for s_N or it could be left as a calibration parameter. The nucleation criterion of Chu and Needleman [15] has now been significantly improved in all respects, particularly for the modelling of particle cracking where the parameters can be readily obtained from a basic metallographic analysis. Alternatively, these nucleation parameters could be calibrated and then compared with the experimental values for these quantities to ensure that they are physically possible.

6.2 Influence of the particle shape on void growth, stress triaxiality and shape evolution

The secondary benefit of the loosely coupled damage model is that the reinforcing influence of the second-phase particles and inclusions can be removed from the bulk material to determine the stress state within the matrix material for improved modelling of void evolution. It is important to note that the traditional damage-based model would give similar predictions of void evolution if the flow stress relation of the matrix was pre-determined from an experimental or numerical procedure. The coupled-GT model not only eliminates this step but also provides the stress state in the matrix and the particles/inclusions as a function of their shape and composition. To elucidate the performance of the coupled-GT model, the standard GT model described in the previous section is evaluated without accounting for the influence of the particles. The improvement of the coupled model is then measured using the results of the standard GT model as the performance baseline. The aspect ratio of the reinforcing particles is varied from 1/6 to 6 to assess the sensitivity of the damage response to a change in the particle geometry.

The inclusion shape has a dramatic influence upon void growth within the bulk material as seen in Fig. 6 where the porosity can reach a percent difference of 50 % or higher for the ellipsoidal particles (oblate and prolate) than if the particles were neglected. The spherical particles will also lead to increased void growth but it is milder in comparison. As noted by Tandon and Weng [18], both the oblate and prolate particles are similar in their ability to reinforce the material with oblate particles or discs providing the best reinforcement shape. It is important to observe the multiplying effect of the particles on void growth as a 10 % volume fraction of particles may yield a significantly larger increase in the predicted void damage.

The trends for the void growth are related to the void aspect ratio and the stress triaxiality in the matrix. From inspection of the stress triaxiality in Fig. 7, the matrix triaxiality is the highest for oblate particles and the lowest for the spherical particles. The better the reinforcing properties of the particles (higher load sharing with the matrix), the more the stress state within the matrix is altered. In fact, the stress triaxiality within the elastic particles decreases as the particle shape changes from spherical to oblate. Therefore, the triaxiality in the matrix must increase to maintain equilibrium. Void evolution is extremely sensitive to the stress triaxiality,

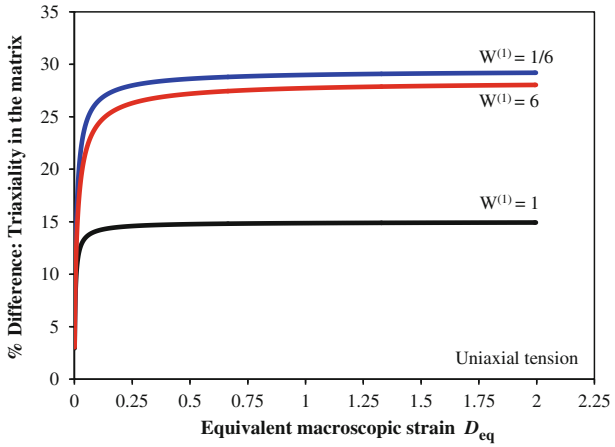

Fig. 7 Influence of the particle shape on the stress triaxiality within the matrix material compared with the standard model where the triaxiality is constant at a value of 1/3. The trends are similar for plane-strain and equal-biaxial tensile loading

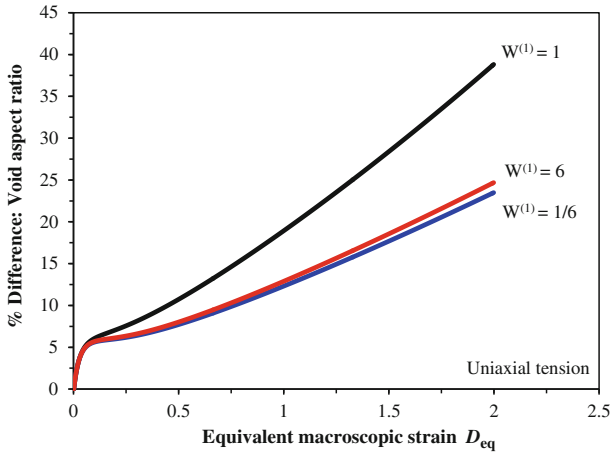

Fig. 8 Influence of the particle shape on the evolution of the void shape in the coupled constitutive model relative to the void shape predicted using the standard GT model without particles. The trends are similar for plane-strain and equal-biaxial tensile loading

and it is this increased stress triaxiality in the matrix that drives void growth as a function of the particle shape. The higher the stress triaxiality, the faster the void growth rate, although void shape effects also play a role and are linked to the triaxiality.

In Fig. 8, it can be seen that the effect of the particle shape on the evolution of the void aspect ratio is opposite to that of void growth since the material reinforced with spherical particles results in the highest shape change. The influence of the particle shape on the matrix triaxiality is also responsible for the decreased shape evolution in the ellipsoidal particle composites. The higher the triaxiality, the more void growth will occur laterally, decreasing the void aspect ratio. In uniaxial tension where the stress triaxiality is 1/3, the void elongates in the loading direction and contracts laterally as the void becomes prolate and eventually needle-like. Since the spherical particles are least effective at increasing the triaxiality in the matrix, the voids will experience the most elongation, and the least growth compared with a composite reinforced with ellipsoidal particles. The trends for the porosity in Fig. 6 are also related to the void shape effects caused by the particles since prolate voids grow slowly in uniaxial tension. The influence of the particles creates a positive-feedback loop where the stress triaxiality is altered, changing the void growth and shape. The void shape in turn affects the growth rate while the increased porosity softens the material, promoting additional growth. In the case of the material containing spherical particles in uniaxial tension, void growth is slowed as the shape evolves to become prolate.

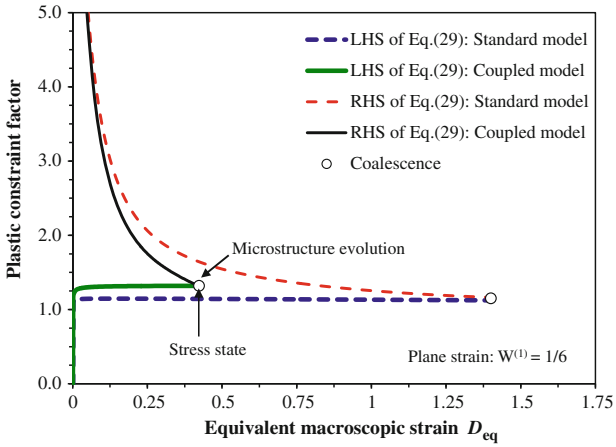

Fig. 9 Variation of the plastic limit load required for coalescence in the coupled and standard (no particles) damage-based constitutive models. The trends are similar for uniaxial and equal-biaxial tensile loading. The influence of the particle shape on the predicted coalescence strain is similar for the spherical and prolate particles since they also promote void evolution and a more severe stress state in the matrix compared with the standard GT constitutive model

6.3 Evaluation of the role of the particles in predicting void coalescence in the standard and coupled damage-based constitutive models

Due to the coupled nature of the model, the resulting inter-relationships may not be immediately apparent but the net effect of the interactions can be observed in the coalescence model. The plastic limit-load criterion in Eq. (29) is a powerful coalescence model since it relates the geometry of the microstructure on the right-hand side (RHS) of the equation to that of the stress state in the material on the left-hand side (LHS). As shown in Fig. 9 for plane-strain loading, the net effect of the particles and voids on the stress state in the matrix shifts the stress state upwards to a more severe one. This stress state results in the evolution of the microstructure through the void volume fraction, aspect ratio and spacing ratio. As the microstructure evolves, the energy required to achieve a localized deformation mode decreases which shifts the plastic constraint to the left in Fig. 9. The intersection of the geometric plastic constraint with the stress state signifies the onset of coalescence and fracture. The highly coupled nature of the model is revealed in Fig. 9 as void coalescence and fracture does not occur in the standard damage-based model until a very high strain while the coupled model predicts fracture at a much more modest strain.

7 Conclusion

An approximate integration scheme has been presented to implement a secant-based homogenization theory for particle-reinforced plasticity into an existing damage-based constitutive model for ductile fracture. The resulting model can account for the influence of the second-phase particles on void growth, shape evolution, coalescence and material softening. The stress state within particles can also be determined as a function of the particle content, shape and elastic properties in order to improve the modelling of nucleation. Additionally, the stress state within the matrix material can be estimated with no prior knowledge of its hardening profile. A significant contribution of this work is that the physical foundation of Gurson-based constitutive models was improved without introducing any additional heuristic or calibration parameters. The present model is best suited for application to sheet metal forming of damage-sensitive industrial alloys where the loading is proportional. A similar methodology as described in this paper could be employed to implement a tangent-based homogenization scheme to extend the coupled model to arbitrary loading conditions.

Acknowledgments Financial support for this work has been provided by the Natural Sciences and Engineering Research Council of Canada (NSERC), the Canada Foundation for Innovation (CFI), the New Brunswick Innovation Foundation (NBIF) and the Auto21 Network of Centers of Excellence, and is gratefully acknowledged. The insightful comments on the manuscript by the anonymous reviewers are also highly appreciated.

References

1. Zhang, Z., Niemi, E.: Studies on the ductility predictions by different local failure criteria. Eng. Fract. Mech. **48**, 529–540 (1994)
2. Zhang, Z., Niemi, E.: Analyzing ductile fracture using dual dilational constitutive equations. Fatig. Fract. Eng. Mater. Struct. **17**, 695–707 (1994)
3. Gologanu, M., Leblond, J.-B., Perrin, G., Devaux, J.: Recent extensions of Gurson's model for porous ductile metals. In: Suquet, P. (ed.) Continuum Micromechanics, pp. 61–130. Springer, New York (1997)
4. Pardoen, T., Hutchinson, J.W.: An extended model for void growth and coalescence. J. Mech. Phys. Solids **48**, 2512–2567 (2000)
5. Zhang, Z., Thaulow, C., Odegard, J.: A complete Gurson model approach for ductile fracture. Eng. Fract. Mech. **67**, 155–168 (2000)
6. Benzerga, A.A.: Micromechanics of coalescence in ductile fracture. J. Mech. Phys. Solids **50**, 1331–1362 (2002)
7. Pardoen, T.: Numerical simulation of low stress triaxiality ductile fracture. Comput. Struct. **84**, 1641–1650 (2006)
8. Lassance, D., Scheyvaerts, F., Pardoen, T.: Growth and coalescence of penny-shaped voids in metallic alloys. Eng. Fract. Mech. **73**, 1009–1034 (2006)
9. Pardoen, T.: Numerical simulation of low stress triaxiality ductile fracture. Comp. Struct. **84**, 1641–1650 (2006)
10. Fabregue, D., Pardoen, T.: A constitutive model for elastoplastic solids containing primary and secondary voids. J. Mech. Phys. Solids **56**, 719–741 (2008)
11. Scheyvaerts, F., Pardoen, T., Onck, P.R: A new model for void coalescence by internal necking. Int. J. Dam. Mech. **19**, 95–126 (2010)
12. Gurson, A.L.: Continuum theory of ductile rupture by void nucleation and growth—part I. Yield criteria and flow rules for porous ductile media. J. Eng. Mater. Technol. **99**, 2–15 (1977)
13. Tvergaard, V.: Influence of voids on shear band instabilities under plane strain conditions. Int. J. Fract. **17**, 389–407 (1981)
14. Beremin, F.M.: Cavity formation from inclusions in ductile fracture of A508 steel. Metall. Trans. A **12**, 723–731 (1981)
15. Chu, C.C., Needleman, A.: Void nucleation effects in biaxially stretched sheets. J. Eng. Mater. Technol. **102**, 249–256 (1980)
16. Berveiller, M., Zaoui, A.: An extension of the self-consistent scheme to plastically-flowing polycrystals. J. Mech. Phys. Solids **26**, 325–344 (1979)
17. Weng, G.J.: Some elastic properties of reinforced solids, with special reference to isotropic ones containing spherical inclusions. Int. J. Eng. Sci. **22**, 845–856 (1984)
18. Tandon, G.P., Weng, G.J.: Average stress in the matrix and effective moduli of randomly oriented composites. Compos. Sci. Tech. **27**, 111–132 (1986)
19. Tandon, G.P., Weng, G.J.: A theory of particle-reinforced plasticity. J. Appl. Mech. **55**, 126–135 (1988)
20. Suquet, P.: Effective properties of nonlinear composites. In: Continuum Micromechanics. CISM Course and Lecture Notes, pp. 197–264 (1997)
21. Hill, R.: Continuum micro-mechanics of elastoplastic polycrystals. J. Mech. Phys. Solids **13**, 89–101 (1965)
22. Gonzalez, C., Segurado, J., Llorca, J.: Numerical simulation of elasto-plastic deformation of composites: evolution of stress microfields and implications for homogenization models. J. Mech. Phys. Solids **52**, 1573–1593 (2004)
23. Doghri, I., Ouaar, A.: Homogenization of two-phase elasto-plastic composite materials and structures: study of cyclic plasticity and numerical algorithms. Int. J. Solids Struct. **40**, 1681–1712 (2003)
24. Christensen, R.M.: A critical evaluation of a class of micro-mechanical models. J. Mech. Phys. Solids **38**, 379–404 (1990)
25. Ponte-Castaneda, P.: The effective mechanical properties of nonlinear isotropic composites. J. Mech. Phys. Solids **39**, 45–71 (1991)
26. Kailasam, M., Ponte Castaneda, P.: A general constitutive theory for linear and nonlinear particulate media with microstructure evolution. J. Mech. Phys. Solids **46**, 65–427 (1998)
27. Ponte-Castaneda, P., Suquet, P.: Nonlinear composites. Adv. Appl. Mech. **34**, 171–301 (1998)
28. Chaboche, J.L., Kanoute, P., Roos, A.: On the capabilities of mean-field approaches for the description of plasticity in metal-matrix composites. Int. J. Plast. **21**, 1409–1434 (2005)
29. Pierard, O., Gonzalez, C., Segurado, J., Llorca, J., Doghri, I.: Micromechanics of elasto-plastic materials reinforced with ellipsoidal inclusions. Int. J. Solids Struct. **44**, 6945–6962 (2007)
30. Mueller, R., Mortensen, A.: Simplified prediction of the monotonic uniaxial stress–strain curve of non-linear particulate composites. Acta Mater. **54**, 2145–2155 (2006)
31. Mori, T., Tanaka, K.:: Average stress in matrix and average elastic energy of materials with misfitting inclusions. Acta Metall. **21**, 571–574 (1973)
32. Butcher, C. (2011) A multi-scale damage percolation model of ductile fracture. Ph.D. thesis, University of New Brunswick, Canada. http://dspace.hil.unb.ca:8080/handle/1882/35391
33. Eshelby, J.D.: The determination of the elastic field of an ellipsoidal inclusion, and related problems. Proc. R. Soc. Lond. A **241**, 376–396 (1957)
34. Ragab, A.R.: Application of an extended void growth model with strain hardening and void shape evolution to ductile fracture under axisymmetric tension. Eng. Fract. Mech. **71**, 1515–1534 (2004)
35. Thomason, P.F.: Ductile Fracture of Metals. Pergamon Press, Oxford (1990)
36. Tohgo, K., Mochizuki, K.: Damage mechanics approach to material-dependency of fracture toughness in aluminum alloys. Int. J. Dam. Mech. **11**, 151–170 (2002)
37. Worswick, M.J., Pelletier, P.: Numerical simulation of ductile fracture during high strain rate deformation. Eur. Phys. J. Appl. Phys. **4**, 257–267 (1998)
38. Butcher, C., Chen, Z.T.: Characterizing void nucleation in a damage-based constitutive model using notched tensile sheet specimens. Theor. Appl. Fract. Mech. **55**, 140–147 (2011)
39. Needleman, A.: Continuum model for void nucleation by inclusion debonding. J. Appl. Mech. **54**, 525–531 (1987)

40. Moulin, N., Jeulin, D., Klöcker, H.: Stress concentrations in non-convex elastic particles embedded in a ductile matrix. Int. J. Eng. Sci. **47**, 170–191 (2009)
41. Griffith, A.A.: The phenomena of rupture and flow and solids. Phil. Trans. R. Soc. Lond. A **221**, 163–198 (1921)